INORGANIC CHEMISTRY FRONTIERS

RESEARCH ARTICLE

View Article Online
View Journal | View Issue

Check for updates

Cite this: *Inorg. Chem. Front.*, 2023, **10**, 1119

γ-$P_4S_3I_2$: a new metal-free infrared second-order nonlinear optical crystal designed by polymorphism strategy†

Xin Zhao, [a,b] Chensheng Lin, [a] Shunda Yang,[a] Haotian Tian,[a,b] Chao Wang,[a,b] Tao Yan, *[a,d] Jian Zhang, [d] Bingxuan Li,[a] Ning Ye[c] and Min Luo *[a]

Received 31st October 2022,
Accepted 16th December 2022

DOI: 10.1039/d2qi02313j

rsc.li/frontiers-inorganic

A non-centrosymmetric metal-free thiophosphate, γ-$P_4S_3I_2$, was successfully synthesized utilizing polymorphism strategy in this study. γ-$P_4S_3I_2$ crystallized in the space group of $P4_3$ and featured paralleled $(P_4S_3I_2)_n$ molecular clusters. Importantly, it exhibited promising nonlinear optical (NLO) performances, such as a phase-matchable second harmonic generation (SHG) efficiency (0.5 × $AgGaS_2$), wide band gap (2.38 eV), large birefringence (0.118@2050 nm), and wide infrared transparency, suggesting that γ-$P_4S_3I_2$ may be a potential IR NLO candidate.

Introduction

Exploring non-centrosymmetric (NCS) inorganic compounds is of great significance in the development of piezoelectric, pyroelectric, ferroelectric, and especially nonlinear optical (NLO) materials.[1–6] NLO materials are indispensable for applications in medical treatment, atmospheric detection and optical communication relying on frequency conversion.[7,8] To date, many well-known NLO crystals, such as β-BaB_2O_4, LiB_3O_5 and $CsLiB_6O_{10}$ as well as $KTiOPO_4$ and $LiNbO_3$, have basically met the needs in the UV and visible (vis) regions.[9–12] However, commercially available NLO crystals used in the infrared (IR) region are still inhibited by some intrinsic drawbacks, such as the poor laser damage threshold (LDT) of $AgGaS_2$ and $AgGaSe_2$ and the two-photon absorption (TPA) of $ZnGeP_2$,[13] which have restricted their further practical applications. Therefore, exploring new IR NLO crystals is still of current research interest.

Generally, inorganic crystals possess a strict structurally non-centrosymmetric space group, which is the prerequisite for NLO materials. However, about 70% of inorganic compounds are crystallize in centrosymmetric space groups,[14] which indicates that NCS compounds are not easily accessible. Thus, some strategies, including chemical substitution, mixing anions and salt-inclusion, have been proposed to obtain NCS compounds, which have resulted in plenty of IR NLO crystals being obtained, such as Li_2ZnSiS_4 (3.9 eV, 1.1 × $AgGaS_2$), Pb_4SeBr_6 (2.62 eV, 1.3 × $AgGaS_2$), $Pb_{18}O_8Cl_{15}I_5$ (2.82 eV, 1.05 × $AgGaS_2$) and $Li[LiCs_2Cl][Ga_3S_6]$ (4.18 eV, 0.7 × $AgGaS_2$).[15–18] Recently, polymorphous modification has been regarded as an effective strategy for exploring new IR NLO crystals, which has been attributed to the following reasons: (i) polymorphism is a common phenomenon in crystalline materials; and (ii) the arrangement of the building units in the structure can be further optimized, which might enhance the SHG effect, for example, $[Ga_4Se_{11}]$ C_2-type supertetrahedra in α-$BaGa_4Se_7$ can be reconstituted to T_2-type $[Ga_4Se_{10}]$ supertetrahedra in β-$BaGa_4Se_7$ with a stronger SHG response.[19] Until now, during the process of exploring new NLO polymorphism, most attention has been focused on borates and Pb-based compounds because the variable architectures of $[B_xO_y]$ and the flexible coordination environment of the Pb^{2+} cation (2–10) were found to be favorable in forming polymorphs.[20,21] Thus, many polymorphous borates and Pb-based compounds were reported, such as α-$BaB_4O_5F_4$, α-$BaBOF_3$, α-$LiPbB_9O_{15}$ and β-$PbGa_2S_4$.[22–25] Moreover, using additives and adjusting temperatures were also helpful to obtain new polymorphs, for instance, β-$Sc(IO_3)_3$ [26] can be obtained with Li_2CO_3 as an additive. Besides, β- and γ-$BaGa_4S_7$, β-$BaGa_4Se_7$ and β-$BaGa_2Se_4$ [27,28] can be synthesized at differing appropriate temperatures. In this study, we proposed thiophosphates as a new system to explore NLO polymorphism.

[a]*Key Laboratory of Optoelectronic Materials Chemistry and Physics, Fujian Institute of Research on the Structure of Matter, Chinese Academy of Sciences, Fuzhou, Fujian 350002, China. E-mail: lm8901@fjirsm.ac.cn, yantao@fjirsm.ac.cn*
[b]*University of Chinese Academy of Sciences, Beijing 100049, China*
[c]*Tianjin Key Laboratory of Functional Crystal Materials, Institute of Functional Crystal, Tianjin University of Technology, Tianjin 300384, China*
[d]*State Key Laboratory of Crystal Materials, Shandong University, Jinan, 250100, China*

†Electronic supplementary information (ESI) available: Crystallographic data, measurements of physical properties, and theoretical calculations. CCDC 2216006. For ESI and crystallographic data in CIF or other electronic format see DOI: https://doi.org/10.1039/d2qi02313j

Thiophosphates are a very promising system for mid-IR NLO applications because the existence of strong covalent P–S bonds not only improves the NLO response but can also drive the blue shift of the short-wave absorption edge;[29] for example, $Hg_3P_2S_8$ (2.72 eV, 4.2 × $AgGaS_2$), $Eu_2P_2S_6$ (2.54 eV, 0.9 × $AgGaS_2$), $RbBiP_2S_6$ (2.10 eV, 11.9 × $AgGaS_2$) and $CuHgPS_4$ (2.03 eV, 6.5 × $AgGaS_2$) exhibit good IR-NLO performances.[30–33] In addition, positive valence P atoms have a flexible coordination environment (2–4), which is favorable in forming polymorphs. For example, the polymorphism of P_2S_7 (α: $P2_1/c$, β: $P\bar{1}$)[34] exhibits two different crystal structures. Moreover, until now, there have been no studies on the NLO properties of metal-free thiophosphates, and thus, we have a strong interest in studying the title compound. Therefore, in this work, we have focused on the P–S–I system and a new non-centrosymmetric polymorph of $P_4S_3I_2$ was discovered and named γ-$P_4S_3I_2$, with the previously reported phases named as α-$P_4S_3I_2$ ($P\bar{1}$) and β-$P_4S_3I_2$ (*Pnma*).[35,36] γ-$P_4S_3I_2$ was successfully synthesized *via* solution evaporation at low temperature, and its linear and nonlinear optical properties were studied experimentally and theoretically. Results show that this compound exhibits a suitable SHG response (0.5 × $AgGaS_2$), wide transparency window, and large birefringence (0.118@2050 nm), indicating that γ-$P_4S_3I_2$ is a promising mid-IR NLO candidate.

Experimental section

Synthesis and crystal growth

All of the chemicals, carbon disulfide CS_2 (99.9%), S (99.99%), P (99.99%) and I_2 (99.99%), were purchased from Shanghai Aladdin Biochemical Technology Co., Ltd and used without further purification. The synthesis of γ-$P_4S_3I_2$ was operated in two steps. First, P_4S_3 was prepared by heating a stoichiometric mixture of P and S in an evacuated silica tube at 300 °C for 24 h. Second, P_4S_3 and I_2 were evenly mixed with a ratio of 1 : 1 and loaded into an evacuated silica tube and then sealed under vacuum. After that, the mixture was heated to 180 °C in a drying oven, held for about 2 days, and then cooled to room temperature naturally, whereupon molten $P_4S_3I_2$ was obtained. γ-$P_4S_3I_2$ was prepared by recrystallizing amorphous $P_4S_3I_2$ in CS_2 at −10 °C. The millimeter-sized crystal of γ-$P_4S_3I_2$ was grown directly by an evaporation method. The recrystallized γ-$P_4S_3I_2$ (1.5 g) was dissolved in dried CS_2 (12 ml) in a round bottom centrifuge tube with a cover, and then the centrifuge tube was put into a refrigerator at −30 °C and held for about 5 days; the products were pure deep yellow block-shaped single crystals without byproducts.

Single crystal structure determination

Single crystal X-ray diffraction data for γ-$P_4S_3I_2$ were collected on a Rigaku Mercury CCD diffractometer with graphite-monochromatic Mo Kα radiation (λ = 0.71073 Å) at room temperature. Some γ-$P_4S_3I_2$ crystals were cut into appropriate sizes on a slide; for measurements, a high-quality single crystal was selected and mounted on top of a glass fiber using epoxy. The intensity data were corrected using a narrow-frame method in ω-scan mode. All data were integrated based on the CrystalClear program. The intensities were corrected for Lorentz polarization, air absorption, and absorption attributable to variation in the path length through the detector faceplate. Absorption corrections were also achieved by using a multi-scan technique. The crystal structures were determined by means of the direct methods and refined by full-matrix least-squares fitting on F^2 using SHELXL.[37,38] All the atoms were refined with anisotropic displacement parameters. The ADDSYM algorithm from the PLATON program[39] was used to monitor the correctness of the structures and no higher symmetry was found. Relevant crystallographic data and details of the experimental conditions are listed in Table S1.† Besides, the data of atomic coordinates and equivalent isotropic displacement parameters, selected bond lengths and angles, and anisotropic displacement parameters are summarized in Tables S2–S4.†

Powder X-ray diffraction

The powder X-ray diffraction analysis of compound γ-$P_4S_3I_2$ was implemented on a Miniflex-600 diffractometer with Cu Kα radiation (λ = 1.540598 Å) at room temperature. The angular range was 2θ = 10–70° with a scan step width of 0.02° and a fixed time of 0.2 s. The powder XRD pattern of polycrystalline materials matched with the calculated XRD pattern from the single crystal model (Fig. S1†), indicating that pure samples could be used for subsequent measurements.

Energy dispersive X-ray spectroscopy (EDS) analysis

The EDS analysis of γ-$P_4S_3I_2$ crystals was carried out on a field emission scanning electron microscope (FESEM, SU-8010) equipped with an energy dispersive X-ray spectrometer. The shaped crystals were rinsed using carbon disulfide and absolute ethyl alcohol, and then were affixed on the copper sample stage with a carbon conductive tape. Different regions on the crystals were tested with a focused beam, accelerating voltage of 20 kV and emission current of 12 μA (Fig. S2†).

Thermal analysis

The thermogravimetric (TG) analysis of γ-$P_4S_3I_2$ was conducted on a Netzsch STA449F3 simultaneous analyzer. The reference (Al_2O_3) and crystal samples (5–10 mg) were enclosed in an Al_2O_3 crucible, heated from 30 to 1000 °C at a rate of 10 °C min^{-1} under a constant flow of nitrogen gas, and then cooled to room temperature naturally.

UV-vis-NIR diffuse reflectance spectroscopy

The UV-vis-NIR diffuse reflection data of γ-$P_4S_3I_2$ were collected on a PerkinElmer Lamda-950 ultraviolet/visible/near-infrared spectrophotometer at room temperature in the range of 400–800 nm with $BaSO_4$ as the standard of 100% reflectance. The reflectance values were converted to absorbance based on the Kubelka–Munk function $F(R) = (1 - R)^2/(2R) = K/S$, where R is the reflectance, K is the absorption, and S is the scattering.[40,41]

Fourier-transform infrared (FT-IR) spectroscopy

The Fourier-transform infrared (FT-IR) transmittance spectra were measured on a Bruker VERTEX 70 FT-IR spectrophotometer in the range of 4000–400 cm^{-1}. Dry KBr was ground into fine powder and then pressed into a transparent wafer as the reference. The powder sample and dry KBr were mixed and pressed into the same wafer for the measurements.

Powder SHG and LDT measurements

Polycrystalline SHG responses were measured using the Kurtz–Perry method[42] with a Q-switched Nd:YAG solid-state laser at a laser radiation wavelength of 2050 nm. Polycrystalline γ-$P_4S_3I_2$ was ground and sieved into several different particle size ranges of 25–45, 45–63, 63–74, 74–106, 106–150, and 150–210 μm. Polycrystalline $AgGaS_2$ was also ground and sieved into the same particle size ranges as the reference. After that, samples were added into aluminous holders and pressed into 1 mm thick slides between two glass sheets bound with a 2 mm thick rubber ring, containing an 8 mm diameter hole in the center. Subsequently, the samples were then placed in a light-tight box and under the irradiation of a pulsed laser. The intensities of the SHG signals were measured with a photomultiplier tube attached to a RIGOL DS1052E 50 MHz oscilloscope. As a result, the ratio of the intensity of the SHG signals between the samples and the reference can eventually be calculated. The laser damage threshold (LDT) measurement was executed at room temperature using microcrystal samples of γ-$P_4S_3I_2$ and $AgGaS_2$ samples of similar sizes (150–212 μm) under a pulsed Nd:YAG laser (1064 nm, 1 Hz, 10 ns). The LDT was evaluated through increasing the energy of the laser gradually until the damage spot was observed. The value of the LDT can be calculated based on eqn (1):

$$I_{(\text{threshold})} = E/(\pi r^2 t) \quad (1)$$

where E, r, and t are the laser damage energy of a single pulse, the spot radius and the pulse width, respectively. Detailed data are listed in Table S5.†

Computational methods

The first-principles calculations for the physical properties of γ-$P_4S_3I_2$ were performed by using CASTEP,[43] a plane-wave pseudopotential total energy package based on density functional theory (DFT).[44] The exchange and correlative potential of electron–electron interactions were represented by generalized gradient approximation (GGA) in the scheme of Perdew–Burke–Ernzerhof (PBE).[45] Furthermore, the interaction of the electrons with ion cores was represented by the norm-conserving pseudopotentials, and the valence electrons were expressed as P: $3s^2$ $3p^3$, S: $3s^2$ $3p^3$ and I: $5s^2$ $5p^5$. The k-point of the first Brillouin zone for γ-$P_4S_3I_2$ was sampled as the 2 × 2 × 1 Monkhorst–Pack scheme,[46] which was used to calculate the optical properties and density of states (DOS). The cut-off energy was set to be 650 eV and the self-consistent convergence of the total energy was 1.0×10^{-5} eV per atom. The scissor operation was adopted in the dielectric function calculation owing to the inherent underestimation of the band gap by the DFT method. In addition, the "velocity-gauge"[47,48] formula was employed to calculate the SHG coefficients of γ-$P_4S_3I_2$, and the SHG density of d_{33} was calculated by the band-resolved method.[49]

Results and discussion

Structural description and comparison

γ-$P_4S_3I_2$ crystallized in the tetragonal crystal system with an asymmetric space group of $P4_3$ (no. 78), with a = 7.3415(2) Å, b = 7.3415(2) Å, and c = 39.1942(19) Å (crystallographic details are shown in Tables S1–S4†). As shown in Fig. 1a, the basic building unit (BBU) of γ-$P_4S_3I_2$ was a unique molecular cluster

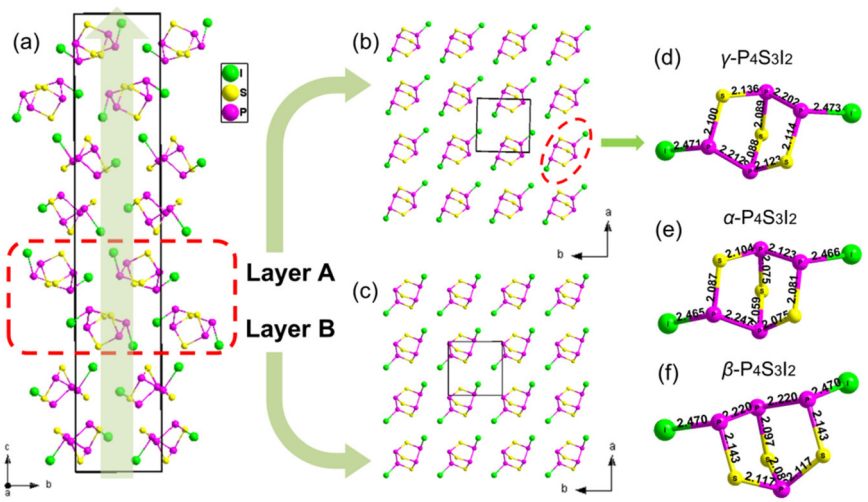

Fig. 1 Crystal structure of γ-$P_4S_3I_2$ viewed along the a-axis (a). Layer A of the $(P_4S_3I_2)_n$ basic building unit in γ-$P_4S_3I_2$ (b). Layer B of the $(P_4S_3I_2)_n$ basic building unit in γ-$P_4S_3I_2$ (c). $P_4S_3I_2$ molecules in γ-$P_4S_3I_2$ (d), α-$P_4S_3I_2$ (e) and β-$P_4S_3I_2$ (f).

$(P_4S_3I_2)_n$ (n = 4) constructed from $P_4S_3I_2$ molecules with two-dimensional (2D) layers (layer A and layer B). The BBUs in γ-$P_4S_3I_2$ were arranged along the c direction with C_4 symmetry and the 4_3 screw axis is paralleled to the c-axis. In addition, layers A and B in the $(P_4S_3I_2)_n$ molecular cluster were interconnected through weak van der Waals interactions between the two layers, and both layers were constructed by using the paralleled $P_4S_3I_2$ molecules in the a–b plane, where adjacent $P_4S_3I_2$ molecules are connected with each other also *via* van der Waals interactions (Fig. 1b and c). The boat-like $P_4S_3I_2$ molecule in γ-$P_4S_3I_2$ contained four P atoms, three S atoms and two I atoms with the I–P bonds ranging from 2.471(3) to 2.480(3) Å, the P–S bonds ranging from 2.082(5) to 2.136(5) Å and the P–P bonds ranging from 2.202(5) to 2.212(5) Å, which are comparable to I–P bonds, P–S bonds and P–P bonds in α-$P_4S_3I_2$ and β-$P_4S_3I_2$.[35,36] Moreover, the structural feature of the boat-like $P_4S_3I_2$ molecules in γ-$P_4S_3I_2$ was similar to that in α-$P_4S_3I_2$, yet quite different from that in β-$P_4S_3I_2$ (Fig. 1d, c and e). The $P_4S_3I_2$ molecules in γ-$P_4S_3I_2$ and α-$P_4S_3I_2$ both showed C_2 local symmetry, while the molecules in β-$P_4S_3I_2$ exhibited C_s local symmetry.

To better understand the structure of γ-$P_4S_3I_2$, α-$P_4S_3I_2$ was chosen to compare with γ-$P_4S_3I_2$ (Fig. 2) because their $P_4S_3I_2$ molecules have the same local symmetry. The structural evolution of γ-$P_4S_3I_2$ could be regarded as that where $P_4S_3I_2$ molecules in α-$P_4S_3I_2$ (Fig. 2a) were partially picked out and regularly rearranged according to a new symmetry, leading to γ-$P_4S_3I_2$, which crystallizes in another space group ($P4_3$). However, as shown in Fig. 2b and c, the distance between the two layers in the $(P_4S_3I_2)_n$ (n = 4) molecular cluster of γ-$P_4S_3I_2$ (4.661 Å) is greater than that of α-$P_4S_3I_2$ (4.648 Å). In addition, the literature values of the van der Waals radii for these atoms are 2.15 Å for I and 1.90 Å for P, which give a sum of 4.05 Å, while the experimental I···P distance in the $(P_4S_3I_2)_n$ (n = 4) molecular cluster of γ-$P_4S_3I_2$ (3.82 Å) and α-$P_4S_3I_2$ (3.87 Å) was considerably less than the sum of their van der Waals radii (Fig. S3†), indicating the existence of intermolecular van der Waals interactions between their $P_4S_3I_2$ molecules.

Thermal analysis

Thermogravimetric (TG) and differential thermal analysis (DTA) curves revealed that γ-$P_4S_3I_2$ was decomposed at 120–300 °C with an exothermic peak at 120 °C (Fig. S5†), indicating that this compound was incongruent. Solid γ-$P_4S_3I_2$ was transformed into liquid amorphous $P_4S_3I_2$ at 120 °C and began to decompose, and γ-$P_4S_3I_2$ can be obtained by recrystallizing the liquid amorphous $P_4S_3I_2$ in CS_2 (Fig. S4†). γ-$P_4S_3I_2$ exhibited considerable thermal stability compared to some metal halide IR NLO crystals, such as $HgBr_2$ (100 °C), $Cs_2Hg_3I_8$–H_2O (110 °C) and $RbHgI_3$ (120 °C).[50–53]

Optical properties

The optical band gap of γ-$P_4S_3I_2$ was determined to be 2.38 eV (Fig. S6†), which is consistent with the deep yellow colour of its crystals. The band gap of γ-$P_4S_3I_2$ is larger than those of some IR NLO thiophosphates, such as $SnPS_3$ (2.35 eV), $RbBiP_2S_6$ (2.10 eV), $CuHgPS_4$ (2.03 eV) and $AgHg_3PS_6$ (1.85 eV).[32,33,54,55] Powder laser damage threshold (LDT) measurements suggested that the LDT of γ-$P_4S_3I_2$ was 11.97 MW cm^{-2}, which was about 2.8 times that of $AgGaS_2$ (4.25 MW cm^{-2}) under the same conditions (Table S5†). In addition, no obvious absorption from 3 to 20 μm was observed in the IR transmittance spectra of γ-$P_4S_3I_2$ (Fig. S7†), indicating that this compound could potentially be applied in the IR region.

NLO properties

According to the anionic group theory, the orientated arrangement of NLO-active structural units is beneficial for achieving a large SHG reponse.[56] Thus, γ-$P_4S_3I_2$ may be expected to exhibit suitable SHG responses because the $(P_4S_3I_2)_n$ (n = 4) molecular clusters were arranged in parallel along the same direction (Fig. 1a). The size-dependent SHG measurements of

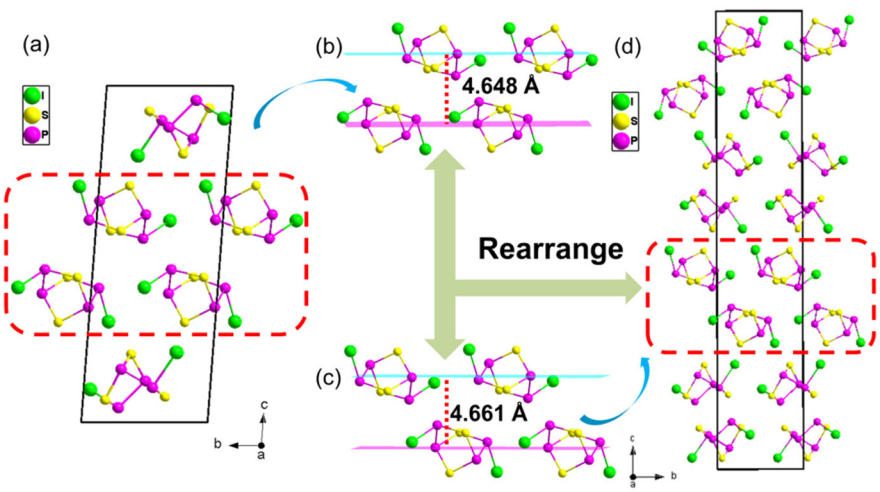

Fig. 2 Crystal structure of α-$P_4S_3I_2$ viewed along the a-axis (a). A $(P_4S_3I_2)_n$ (n = 4) molecular cluster in α-$P_4S_3I_2$ (b). A $(P_4S_3I_2)_n$ (n = 4) molecular cluster in γ-$P_4S_3I_2$ (c). Crystal structure of γ-$P_4S_3I_2$ viewed along the a-axis (d).

the polycrystalline samples of γ-$P_4S_3I_2$ and standard $AgGaS_2$ were performed using a 2.05 μm laser. The intensities of the SHG signals were gradually increased along with an increase of particle sizes (Fig. 3b), indicating that the required type-I phase-matching behavior could be realized in γ-$P_4S_3I_2$. Furthermore, the SHG response of γ-$P_4S_3I_2$ was about 0.5 times that of AGS within the same particle size range of 150–210 μm, which was considerable among some reported IR NLO chalcogenides, such as $SnI_4{\cdot}S_8$ (0.5 × $AgGaS_2$), $CH_3I{\cdot}S_8$ (0.7 × $AgGaS_2$), $LiGa_2PS_6$ (0.5 × $AgGaS_2$), $Rb_2GaP_2S_9$ (0.1 × $AgGaS_2$) and $AgHg_3PS_6$ (0.5 × $AgGaS_2$).[55,57–59] These results demonstrated that γ-$P_4S_3I_2$ had great potential as an IR NLO candidate.

Theoretical calculations

To further understand the electronic structure and optical properties, systematic theory calculations for γ-$P_4S_3I_2$ were performed based on density functional theory (DFT). The calculated band structure suggests that the direct band gap of γ-$P_4S_3I_2$ was 2.123 eV as both the top of the valence band (VB) and the bottom of the conduction band (CB) were located at the X point (Fig. S8†). As can be seen in the partial density of state (PDOS) curves of γ-$P_4S_3I_2$ (Fig. S9†), the top of the valence band was dominated by I 5p, P 3p and S 3p orbitals, and the bottom of the conduction band was also occupied by I 5p, P 3p and S 3p orbitals, indicating that the linear optical properties of γ-$P_4S_3I_2$ were determined by the $P_4S_3I_2$ molecules.

The space group $P4_3$ of γ-$P_4S_3I_2$ belonged to point group 4. According to the Kleinman symmetry, two independent nonzero SHG tensors, d_{31} and d_{33} remained (Fig. S10†). The largest tensor d_{33} value at 2.05 μm in γ-$P_4S_3I_2$ was 9.60 pm V^{-1}, which was about 0.63 times that of $AgGaS_2$ (15.3 pm V^{-1}), matching with the corresponding measured results. In

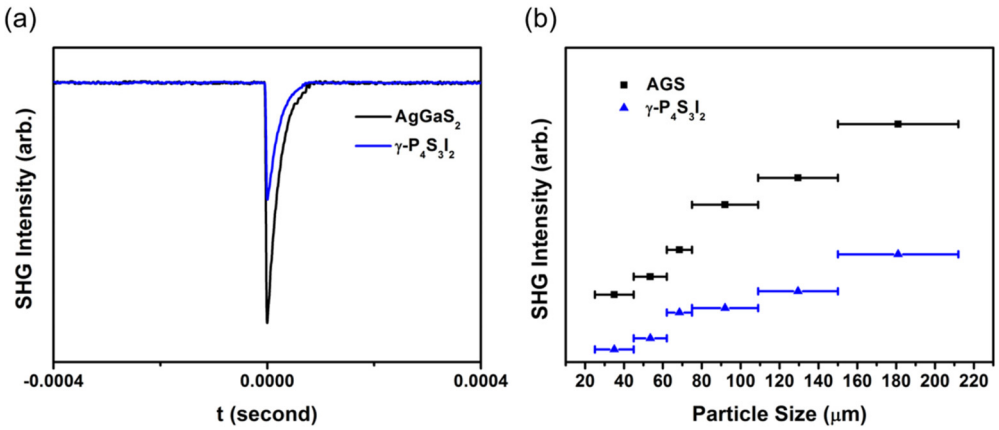

Fig. 3 Measured SHG signals of γ-$P_4S_3I_2$ and $AgGaS_2$ with a 150–210 μm particle size (a). Measured SHG intensities of γ-$P_4S_3I_2$ and $AgGaS_2$ under 2.05 μm laser irradiation at room temperature (b).

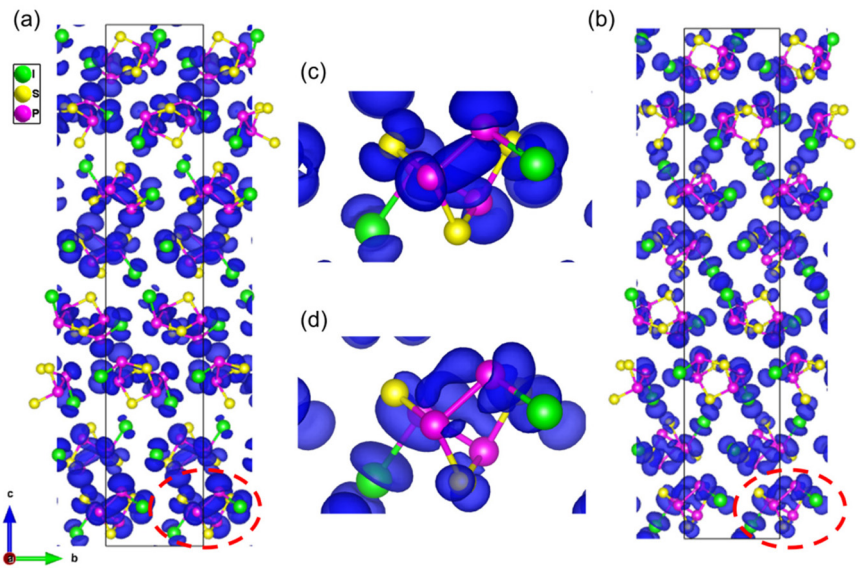

Fig. 4 The SHG-weighted densities for occupied (a, c) and unoccupied (b, d) electronic states in γ-$P_4S_3I_2$.

addition, to clearly illustrate the origin of the contribution of the SHG effect in γ-$P_4S_3I_2$, the SHG-weighted densities of the largest tensor d_{33} were calculated. As shown in Fig. 4, the I atoms, S atoms, P atoms and P–P bonds in the $P_4S_3I_2$ molecule contributed to both occupied and unoccupied electronic states, which confirmed that the $(P_4S_3I_2)_n$ molecular clusters determined the SHG response.

Additionally, the calculated dispersion of the refractive indices curves of γ-$P_4S_3I_2$ is displayed in Fig. S11.† The results were $n_c < n_a$ and the birefringence $(n_c - n_a)$ of γ-$P_4S_3I_2$ was calculated to be 0.118 at 2050 nm, which contributed to the type-I phase-matching behavior over a wide IR region and matched the experimental results. These results indicated that the $P_4S_3I_2$ molecules may be potential fundamental building units for birefringence materials.

Conclusions

In summary, a non-centrosymmetric metal-free thiophosphate, γ-$P_4S_3I_2$, was successfully synthesized and investigated for NLO materials based on polymorphism strategy. The crystal structure of γ-$P_4S_3I_2$ featured paralleled $(P_4S_3I_2)_n$ molecular clusters connecting with each other through van der Waals interactions. γ-$P_4S_3I_2$ also showed excellent nonlinear optical performances including a suitable SHG response (0.5 × $AgGaS_2$), wide band gap (2.38 eV), large birefringence (0.118@2050 nm), and wide infrared transparency. More importantly, the polymorphism strategy in this work may provide new thoughts for exploring new NLO materials with enhanced properties.

Author contributions

Xin Zhao performed the experiments, data analysis, and paper writing; Shunda Yang and Chao Wang offered help in synthesizing the compounds; Tao Yan and Jian Zhang offered help in analyzing the experimental data; Chensheng Lin and Haotian Tian performed the theoretical calculations; Bingxuan Li performed the powder laser damage threshold (LDT) measurements; Min Luo revised the manuscript. Ning Ye and Min Luo guided and supervised the experiments. All authors contributed to the general discussion.

Conflicts of interest

There are no conflicts to declare.

Acknowledgements

This work was supported by the National Natural Science Foundation of China (Grant No. 22222510, 21975255 and 21921001), Natural Science Foundation of Fujian Province (2021J01514), the Foundation of Fujian Science & Technology Innovation Laboratory (2021ZR202), Youth Innovation Promotion Association CAS (2019303) and Open Project of State Key Laboratory of Crystal Materials, Shandong University (KF1907).

References

1 C. J. Cui, F. Xue, W. J. Hu and L. J. Li, Two-dimensional Materials with Piezoelectric and Ferroelectric Functionalities, *npj 2D Mater. Appl.*, 2018, **2**, 1–14.
2 L. Gao, J. B. Huang, S. R. Guo, Z. H. Yang and S. L. Pan, Structure-property Survey and Computer-assisted Screening of Mid-infrared Nonlinear Optical Chalcohalides, *Coord. Chem. Rev.*, 2020, **421**, 213379.
3 Z. X. Chen, W. L. Liu and S. P. Guo, A Review of Structures and Physical Properties of Rare Earth Chalcophosphates, *Coord. Chem. Rev.*, 2023, **474**, 214870.
4 W. F. Zhou, B. X. Li, W. L. Liu and S. P. Guo, AAg(2)PS(4) (A = K, Na/K): The First-type of Non-centrosymmetric Alkali Metal Ag-based Thiophosphates Exhibiting Excellent Second-order Nonlinear Optical Performances, *Inorg. Chem. Front.*, 2022, **9**, 4990–4998.
5 Q. Wu, C. Yang, X. Liu, J. Ma, F. Liang and Y. S. Du, Dimensionality Reduction Made High-performance Mid-Infrared Nonlinear Halide Crystal, *Mater. Today Phys.*, 2021, **21**, 100569.
6 F. Xu, G. Zhang, M. Luo, G. Peng, Y. Chen, T. Yan and N. Ye, A Powder Method for The High-efficacy Evaluation of Electro-optic Crystals, *Natl. Sci. Rev.*, 2020, **8**, nwaa104.
7 B. J. Guo, Y. Wang, C. Peng, H. L. Zhang, G. P. Luo, H. Q. Le, C. Gmachl, D. L. Sivco, M. L. Peabody and A. Y. Cho, Laser-based Mid-infrared Reflectance Imaging of Biological Tissues, *Opt. Express*, 2004, **12**, 208–219.
8 L. K. Cheng, W. R. Bosenberg and C. L. Tang, Growth and Characterization of Nonlinear Optical-crystals Suitable for Frequency-conversion, *Prog. Cryst. Growth Charact. Mater.*, 1990, **20**, 9–57.
9 C. T. Chen, Y. C. Wu, A. D. Jiang, B. C. Wu, G. M. You, R. K. Li and S. J. Lin, New Nonlinear-optical Crystal-LiB_3O_5, *J. Opt. Soc. Am. B*, 1989, **6**, 616–621.
10 T. Sasaki, Y. Mori, I. Kuroda, S. Nakajima, K. Yamaguchi, S. Watanabe and S. Nakai, Cesium Lithium Borate-a New Nonlinear-optical Crystal, *Acta Crystallogr., Sect. C: Cryst. Struct. Commun.*, 1995, **51**, 2222–2224.
11 J. D. Bierlein and H. Vanherzeele, Potassium Titanyl Phosphate and New Applications, *J. Opt. Soc. Am. B*, 1989, **6**, 622–633.
12 G. D. Boyd, K. Nassau, R. C. Miller, W. L. Bond and A. Savage, LiB_3O_6-efficient Phase Matchable Nonlinear Optical Material, *Appl. Phys. Lett.*, 1964, **5**, 234–236.
13 D. N. Nikogosyan, *Nonlinear Optical Crystals: a Complete Survey*, Springer-Science and Business Media, New York, 2005.
14 Y. C. Liu, Y. Q. Li, Y. Zhou, Q. R. Ding, Y. X. Chen, S. G. Zhao and J. H. Luo, A New Nonlinear Optical Sulfate

of Layered Structure: $Cs_2Zn_2(SO_4)_3$, *Inorg. Chem. Commun.*, 2021, **124**, 108390.

15 G. M. Li, Y. Chu and Z. X. Zhou, From $AgGaS_2$ to Li_2ZnSiS_4: Realizing Impressive High Laser Damage Threshold Together with Large Second-harmonic Generation Response, *Chem. Mater.*, 2018, **30**, 602–606.

16 J. Wang, H. Wu, H. Yu, Z. Hu, J. Wang and Y. Wu, Pb_4SeBr_6: A Congruently Melting Mid-infrared Nonlinear Optical Material with Excellent Comprehensive Performance, *Adv. Opt. Mater.*, 2022, **10**, 2102673.

17 X. Chen, Q. Jing and K. M. Ok, $Pb_{18}O_8Cl_{15}I_5$: A Polar Iead Mixed Oxyhalide with Unprecedented Architecture and Excellent Infrared Nonlinear Optical Properties, *Angew. Chem., Int. Ed.*, 2020, **59**, 20323–20327.

18 B. W. Liu, X. M. Jiang, B. X. Li, H. Y. Zeng and G. C. Guo, Li $[LiCs_2Cl][Ga_3S_6]$: A Nanoporous Framework of GaS_4 Tetrahedra with Excellent Nonlinear Optical Performance, *Angew. Chem., Int. Ed.*, 2020, **59**, 4856–4859.

19 Z. Qian, Q. Bian, H. P. Wu, H. W. Yu, Z. S. Lin, Z. G. Hu, J. Y. Wang and Y. C. Wu, β-$BaGa_4Se_7$: A Promising IR Nonlinear Optical Crystal Designed by Predictable Structural Rearrangement, *J. Mater. Chem. C*, 2021, **10**, 96–101.

20 S. C. Wang, N. Ye, W. Li and D. Zhao, Alkaline Beryllium Borate $NaBeB_3O_6$ and $ABe_2B_3O_7$ (A = K, Rb) as UV Nonlinear Optical Crystals, *J. Am. Chem. Soc.*, 2010, **132**, 8779–8786.

21 C. M. Huang, F. F. Zhang, S. C. Cheng, Z. H. Yang and S. L. Pan, α-, β-$Pb_4B_2O_7$ and α-, β-$Pb_4B_6O_{13}$: Polymorphism Drives Changes in Structure and Performance, *Sci. China Mater.*, 2020, **63**, 806–815.

22 W. B. Zhang, S. R. Guo, S. J. Han, L. Y. Wang, X. Zhou, Z. H. Yang and S. L. Pan, $BaB_4O_5F_4$ with Reversible Phase Transition Featuring Unprecedented Fundamental Building Blocks of $B_{16}O_{21}F_{16}$ in the α-phase and $B_4O_6F_4$ in the β-phase, *Chem. Commun.*, 2021, **57**, 4182–4185.

23 K. T. Liu, J. Han, T. Baiheti, F. M. Li, Z. L. Wei, Z. H. Yang, M. Mutailipu and S. L. Pan, Finding a Series of $BaBOF_3$ Fluorooxoborate Polymorphs with Tunable Symmetries: A Simple but Flexible Case, *Chem. Mater.*, 2021, **33**, 7905–7913.

24 K. T. Liu, J. Han, F. M. Li, S. J. Han, Z. H. Yang, X. P. Wang and S. L. Pan, α-$LiMB_9O_{15}$ (M = Sr, Pb): Flexible B_3O_7 Units Leading to the Low Temperature Phase of β-$LiMB_9O_{15}$ (M = Sr, Pb), *Inorg. Chem. Front.*, 2022, **9**, 5371–5376.

25 W. F. Chen, B. W. Liu, X. M. Jiang and G. C. Guo, Infrared Nonlinear Optical Performances of a New Sulfide β-$PbGa_2S_4$, *J. Alloys Compd.*, 2022, **905**, 164090.

26 C. Wu, G. F. Wei, X. X. Jiang, Q. K. Xu, Z. S. Lin, Z. P. Huang, M. G. Humphrey and C. Zhang, Additive-Triggered Polar Polymorph Formation: β-$Sc(IO_3)_3$, a Promising Next-Generation Mid-Infrared Nonlinear Optical Material, *Angew. Chem., Int. Ed.*, 2022, **61**, e202208514.

27 Z. Qian, H. N. Liu, Y. J. Zhang, H. P. Wu, Z. G. Hu, J. Y. Wang, Y. C. Wu and H. W. Yu, The Exploration of New Infrared Nonlinear Optical Crystals Based on the Polymorphism of $BaGa_4S_7$, *Inorg. Chem. Front.*, 2022, **9**, 4632–4641.

28 Y. J. Zhang, Q. Bian, H. P. Wu, H. W. Yu, Z. G. Hu, J. Y. Wang and Y. C. Wu, Designing a New Infrared Nonlinear Optical Material, β-$BaGa_2Se_4$ Inspired by the Phase Transition of the BaB_2O_4 (BBO) Crystal, *Angew. Chem., Int. Ed.*, 2022, **61**, e202115374.

29 Z. Li, J. Y. Yao and Y. C. Wu, Chalcophosphates: A Treasure House of Infrared Nonlinear Optical Materials, *Cryst. Growth Des.*, 2020, **20**, 7550–7564.

30 W. H. Xing, F. Liang, C. L. Tang, E. Uykur, Z. S. Lin, J. Y. Yao, W. L. Yin and B. Kang, Highly Distorted HgS_4 Motif-Driven Structural Symmetry Degradation and Strengthened Second-Harmonic Generation Response in the Defect Diamond-Like Chalcogenide $Hg_3P_2S_8$, *ACS Appl. Mater. Interfaces*, 2021, **13**, 37321–37328.

31 X. Huang, S. H. Yang, X. H. Li, W. L. Liu and S. P. Guo, $Eu_2P_2S_6$: The First Rare-Earth Chalcogenophosphate Exhibiting Large Second-Harmonic Generation Response and High Laser-Induced Damage Threshold, *Angew. Chem., Int. Ed.*, 2022, **61**, e202206791.

32 M. M. Chen, S. H. Zhou, W. B. Wei, M. Y. Ran, B. X. Li, X. T. Wu, H. Lin and Q. L. Zhu, $RbBiP_2S_6$: A Promising IR Nonlinear Optical Material with a Giant Second-Harmonic Generation Response Designed by Aliovalent Substitution, *ACS Mater. Lett.*, 2022, **4**, 1264–1269.

33 M. Y. Li, Z. J. Ma, B. X. Li, X. T. Wu, H. Lin and Q. L. Zhu, $HgCuPS_4$: An Exceptional Infrared Nonlinear Optical Material with Defect Diamond-like Structure, *Chem. Mater.*, 2020, **32**, 4331–4339.

34 T. Rodl, R. Weihrich, J. Wack, J. Senker and A. Pfitzner, Rational Syntheses and Structural Characterization of Sulfur-Rich Phosphorus Polysulfides: α-P_2S_7 and β-P_2S_7, *Angew. Chem., Int. Ed.*, 2011, **50**, 10996–11000.

35 D. A. Wright and B. R. Penfold, The Crystal and Molecular Structure of Phosphorus Thioiodide, *Acta Crystallogr., Sect. A*, 1959, **12**, 455–460.

36 G. J. Penney and G. M. Sheldrick, Preparation and Molecular Structure of a New Isomer of $P_4S_3I_2$: 3,5-Di-iodo-2,6,7-trithia-1,3,4,5-tetraphosphabicyclo [2,2,1] heptane, *J. Chem. Soc. A*, 1971, **9**, 1100–1103.

37 G. M. Sheldrick, A Short History of SHELX, *Acta Crystallogr., Sect. A: Found. Crystallogr.*, 2008, **64**, 112–122.

38 G. M. Sheldrick, Crystal Structure Refinement with SHELXL, *Acta Crystallogr., Sect. C: Struct. Chem.*, 2015, **71**, 3–8.

39 A. L. Spek, Single-crystal Structure Validation with The Program PLATON, *J. Appl. Crystallogr.*, 2003, **36**, 7–13.

40 J. Tauc, Absorption Edge and Internal Electric Fields in Amorphous Semiconductors, *Mater. Res. Bull.*, 1970, **5**, 721–730.

41 S. Landi, I. R. Segundo, E. Freitas, M. Vasilevskiy, J. Carneiro and C. J. Tavares, Use and misuse of the

Kubelka-Munk Function to Obtain the Band Gap Energy From Diffuse Reflectance Measurements, *Solid State Commun.*, 2022, **341**, 114573.
42 S. K. Kurtz and T. T. Perry, A Powder Technique for the Evaluation of Nonlinear Optical Materials, *J. Appl. Phys.*, 1968, **39**, 3798–3813.
43 S. J. Clark, M. D. Segall, C. J. Pickard, P. J. Hasnip, M. J. Probert, K. Refson and M. C. Payne, First Principles Methods Using CASTEP, *Z. Kristallogr.*, 2005, **220**, 567–570.
44 W. Kohn, Nobel Lecture: Electronic Structure of Matter-wave Functions and Density Functionals, *Rev. Mod. Phys.*, 1999, **71**, 1253–1266.
45 J. P. Perdew, A. Ruzsinszky, G. I. Csonka, O. A. Vydrov, G. E. Scuseria, L. A. Constantin, X. L. Zhou and K. Burke, Restoring the Density-gradient Eexpansion for Exchange in Solids and Surfaces, *Phys. Rev. Lett.*, 2008, **100**, 136406.
46 H. J. Monkhorst and J. D. Pack, Special Points for Brillouin-zone Integrations, *Phys. Rev. B: Solid State*, 1976, **13**, 5188–5192.
47 D. J. Moss, E. Ghahramani, J. E. Sipe and H. M. Vandriel, Band-structure calculation of dispersion and anisotropy in $\chi^{(3)}$ for third-harmonic generation in Si, Ge, and GaAs, *Phys. Rev. B: Condens. Matter Mater. Phys.*, 1990, **41**, 1542–1560.
48 W. D. Cheng, C. S. Lin, H. Zhang and G. L. Chai, Theoretical Evaluation on Terahertz Source Generators from Ternary Metal Chalcogenides of PbM_6Te_{10} (M = Ga, In), *J. Phys. Chem. C*, 2018, **122**, 4557–4564.
49 M. H. Lee, C. H. Yang and J. H. Jan, Band-resolved Analysis of Nonlinear Optical Properties of Crystalline and Molecular Materials, *Phys. Rev. B: Condens. Matter Mater. Phys.*, 2004, **70**, 235110.
50 T. Liu, J. Qin, G. Zhang, T. Zhu, F. Niu, Y. Wu and C. Chen, Mercury Bromide ($HgBr_2$): A Promising Nonlinear Optical Material in IR Region with a High Laser Damage Threshold, *Appl. Phys. Lett.*, 2008, **93**, 091102.
51 Y. Li, Y. Ding, Y. Li, H. Liu, X. Meng, Y. Cong, J. Zhang, X. Li, X. Chen and J. Qin, Synthesis, Crystal Structure and Nonlinear Optical Property of $RbHgI_3$, *Crystals*, 2017, **7**, 148.
52 Q. Wu, Y. Huang, X. G. Meng, C. Zhong, X. G. Chen and J. G. Qin, Exploration of New Decond-order Nonlinear Optical Materials of the Cs-Hg-Br-I system, *Dalton Trans.*, 2014, **43**, 8899–8904.
53 Q. Wu, C. Yang, J. Ma, X. Liu and Y. J. Li, Halogen-Ion-Induced Structural Phase Transition Giving a Polymorph of $HgBr_2$ with Balanced Nonlinear Optical Properties, *Inorg. Chem.*, 2021, **60**, 19297–19303.
54 Z.-H. Shi, M. Yang, W.-D. Yao, W. Liu and S.-P. Guo, $SnPQ_3$ (Q=S, Se, S/Se): A Series of Lone-Pair Cationic Chalcogenophosphates Exhibiting Balanced NLO Activity Originating from SnQ_8 Units, *Inorg. Chem.*, 2021, **60**, 14390–14398.
55 Y. Wang, Y. Q. Fang, Y. Z. Cao and F. Q. Huang, Two Nonlinear Optical Thiophosphates $Cu_5Hg_{0.5}P_2S_8$ and $AgHg_3PS_6$ Activated by Their Tetrahedra-Stacking Architecture, *Inorg. Chem.*, 2022, **61**, 1620–1626.
56 C. T. Chen, Y. C. Wu and R. K. Li, The Anionic Group Theory of the Non-linear Optical Effect and its Applications in the Development of New High-quality NLO Crystals in the Borate Series, *Int. Rev. Phys. Chem.*, 1989, **8**, 65–91.
57 S.-P. Guo, Y. Chi and H.-G. Xue, $SnI_4{\cdot}(S_8)_2$: A Novel Adduct-Type Infrared Second-Order Nonlinear Optical Crystal, *Angew. Chem., Int. Ed.*, 2018, **57**, 11540–11543.
58 J. H. Feng, C. L. Hu, B. X. Li and J. G. Mao, $LiGa_2PS_6$ and $LiCd_3PS_6$: Molecular Designs of Two New Mid-Infrared Nonlinear Optical Materials, *Chem. Mater.*, 2018, **30**, 3901–3908.
59 Q. C. Hu, K. B. Ruan, Y. Z. Wang, K. Ding and Y. Xu, Synthesis and Nonlinear Optical Properties of New Gallium Thiophosphate $Rb_2Ga_2P_2S_9$, *New J. Chem.*, 2019, **43**, 12468–12474.